Growth Kinetics of Vertically Aligned Carbon Nanotube Arrays in Clean Oxygen-free Conditions

Jung Bin In,[†] Costas P. Grigoropoulos,[†] Alexander A. Chernov,[‡] and Aleksandr Noy[§,⊥,*]

[†]Department of Mechanical Engineering, University of California Berkeley, Berkeley, CA, [‡]Physical and Life Sciences Directorate, Lawrence Livermore National Laboratory, Livermore, CA, [§]School of Natural Sciences, University of California Merced, Merced, CA, and [⊥]The Molecular Foundry, Lawrence Berkeley National Laboratory, Berkeley, CA

ABSTRACT Vertically aligned carbon nanotubes (CNTs) are an important technological system, as well as a fascinating system for studying basic principles of nanomaterials synthesis; yet despite continuing efforts for the past decade many important questions about this process remain largely unexplained. We present a series of parametric ethylene chemical vapor deposition growth studies in a "hot-wall" reactor using ultrapure process gases that reveal the fundamental kinetics of the CNT growth. Our data show that the growth rate is proportional to the concentration of the carbon feedstock and monotonically decreases with the concentration of hydrogen gas and that the most important parameter determining the rate of the CNT growth is the production rate of active carbon precursor in the gas phase reaction. The growth termination times obtained with the purified gas mixtures were strikingly insensitive to variations in both hydrogen and ethylene pressures ruling out the carbon encapsulation of the catalyst as the main process termination cause.

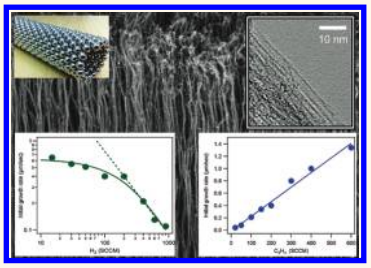

KEYWORDS: carbon nanotube · CVD growth · growth kinetics · impurity removal

Carbon nanotubes (CNTs) have achieved a virtually iconic status in the nanotechnology field because of their unique combination of electrical, mechanical, and electronic properties that seem to embody the promise of a new generation of nanomaterials. Vertically aligned carbon nanotube (VACNT) arrays—forests of parallel aligned nanotubes—could be a key component for applications that range from field emitters and displays,[1] to highly permeable membranes.[2] However, development of these applications has to rely on controllable, economic, and highly tunable synthesis techniques that can produce these arrays reliably on large scale. Chemical vapor deposition (CVD) based methods have established themselves as front-runners for this task from the early stage of nanotube synthesis research,[3] especially after CVD was combined with growth promoters such as water that significantly enhance catalytic lifetime and growth yield.[4,5]

Despite these improvements in synthesis technique for the past decades, understanding of the growth kinetics remains a topic for debate. The process configuration is deceptively simple: most of the thermal CVD processes for nanotube growth involve passing a gas mixture that contains a carbon feedstock gas, a reducing gas (typically hydrogen), and an inert carrier gas over catalytic nanoparticles above the pyrolysis temperature of the carbon feedstock. Qualitatively, it is clear that the carbon source undergoes a series of decomposition steps either in the gas phase or on the catalyst surface, and then incorporates into a growing nanotube. This growth proceeds at a rather high rate (up to several micrometers per second), yielding arrays that could reach 10 mm in height or more,[6,7] and then terminates quickly and often irreversibly. Recent studies have observed significant difference in growth efficiency among hydrocarbon species,[8−12] suggesting that possible pyrolysis or gas phase reactions (GPR) accompanying gas heating on the substrate or reactor wall in CVD can affect growth kinetics.[13−15] Studies targeting the influence of hydrogen in growth kinetics are relatively rare,[16] although its effect on nanotube morphology has been studied extensively.[17−19]

Despite the simplicity of the process, a growing number of papers are reporting different kinetic trends and often-conflicting explanations. To complicate the situation further many studies produce different kinetic trends in different laboratories, despite using similar setups. Although at this

* Address correspondence to anoy@ucmerced, anoy@lbl.gov.

Received for review July 29, 2011 and accepted November 9, 2011.

Published online November 09, 2011
10.1021/nn2028715

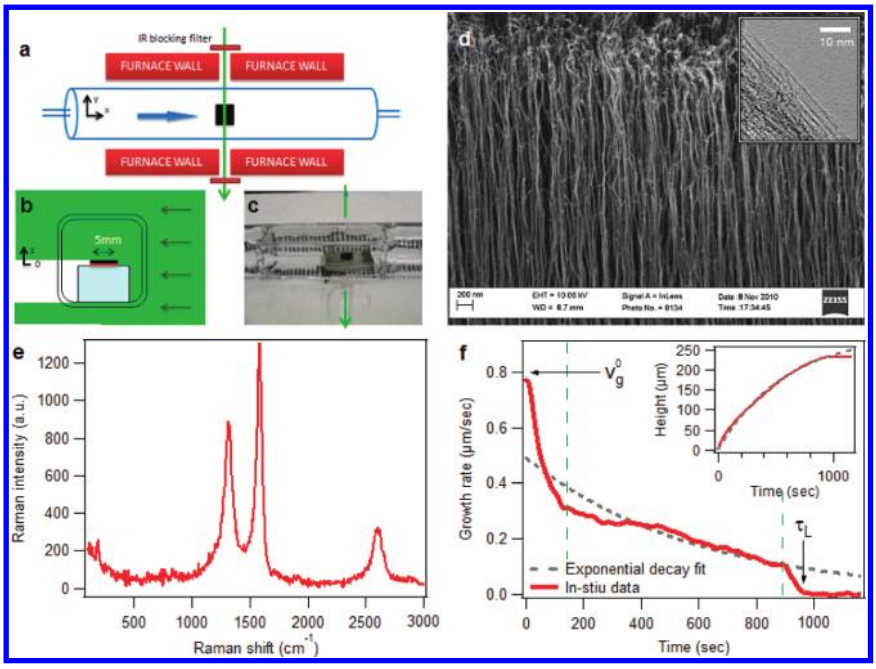

Figure 1. (a) A schematic describing coupling of an *in situ* measurement system with the CNT growth furnace. A narrow slit (2−3 mm) was made through the furnace to allow the beam to illuminate the growing nanotubes. (b) A schematic of cross-sectional view along probing beam. (c) A photo image near the center of the furnace. The green line indicates the beam path. (d) A SEM image of the aligned carbon nanotubes. The inset is a TEM image of the nanotubes after dispersing the nanotubes on a TEM grid. (e) A RAMAN spectrum of the nanotubes grown with 30% ethylene and 40% hydrogen with helium dilution (total 1000 SCCM). (f) A representative kinetic (growth rate−time) curve of the nanotubes of panel e. The initial growth rate (v_g^0) and catalytic lifetime (τ_L) are indicated by arrows. It shows three distinctive regimes designated by green dotted lines. The inset is the corresponding height−time curve.

point the benefit of using additives, such as water, is well established, the mechanism of their action is still not well understood. Finally, another significant aspect of the process, growth termination mechanism, which can provide fundamental clues for synthesis of very long nanotubes, and a catalyst regeneration strategy for low-cost production, remains a source of the lively debate.[14,20−22]

In this paper, we focus on removing the confusing effects of gaseous additives and impurities and revealing the fundamental kinetics of the VACNT growth and termination. We use a CVD growth setup that combined highly purified process gases with an *in situ* growth kinetics monitoring system to characterize this kinetics. We present a generalized model of the CNT growth kinetics and show how it could generate different kinetics reported in the literature. We explore how the major input variables change this "base" kinetics of VACNT growth and, in the central result of this work, we demonstrate that the growth kinetics obeys quite simple and straightforward relationships. Finally, we report the data on the growth termination kinetics and discuss the potential mechanisms for this process.

EXPERIMENTAL DESIGN

Our experiments utilized atmospheric pressure CVD growth setup based on a 1-in. size tube furnace (Figure 1a). This type of setup is commonly used in CNT growth studies; however, our system incorporated two significant modifications. Different molecular forms and concentrations of oxygen-containing species can render the growth chemistry complicated by activating or degrading catalyst.[10,23] We have recently reported that even traces of oxygen-containing gas impurities promote growth and distort the kinetic trends, especially for high-pressure CVD growth.[24] To eliminate these contributions, we have installed high-efficiency gas purifiers on the process gas lines that removed these impurities down to below 1 ppb levels. Another significant addition to the system was the optical micrometer system[24,25] that provided us with capability for *in situ* monitoring of the array growth (see details in the Supporting Information.) In this setup, a telecentric LED beam illuminates the growing nanotubes through a transparent quartz tube, casting a shadow onto a CCD detector (Figure 1a−c). This method provides a nondestructive, noninterfering, fast (1 Hz for this study) and accurate way in measuring height of the VACNTs in real time.[25] However, we found that the surface roughness of a general circular quartz tube distorted the scanning beam of the telecentric optic system, resulting in slightly wavy growth curves; to remedy this problem we have replaced the center section of the process tube with a square 15 mm × 15 mm tube (Quartz Plus, Inc.) with a 60−40 mechanical polish applied to the walls. This setup produces smooth and much more reliable kinetic curves. We also confirmed

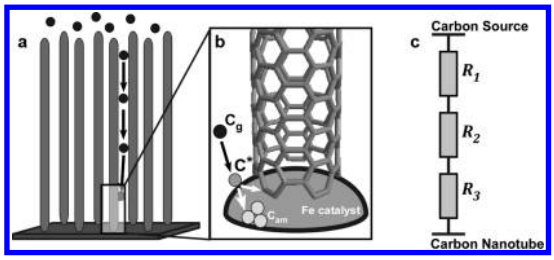

Figure 2. A simplified model of carbon nanotube growth. (a) Diffusion through the CNT array followed by (b) reaction at the catalyst and carbon incorporation into a growing nanotube. (c) Equivalent electrical circuit representing the growth model.

that the difference in catalytic lifetime and the final height of nanotubes was almost negligible between both types of quartz tubes; therefore, the shape change from a round tube to a square tube did not significantly affect CNT growth. We also note that the telecentric optical system only detects the position of the tallest part of the growing CNT array, and thus cannot give a reliable indication of the growth uniformity; however, our postgrowth analysis of the samples showed that the deviations of the final height of the CNT array did not exceed 5%. Moreover, reliability of our measurement is supported by the conclusions of Kim *et al.*,[26] where very similar growth rate curves were obtained by direct measurement after cutting the substrate. Our CNT synthesis followed the procedures described in the previous studies[24] (see also details in the Methods section and in Supporting Information.) To maintain constant initial activity of the catalyst, we have applied identical pretreatment regime during the furnace heating and catalyst reduction, prior to applying the growth gas mixture. In most of the runs we obtained vertically aligned carbon nanotube arrays consisting of a mixture of SWNT and MWNT (Figure 1d). Generally, RAMAN spectra of as-grown nanotubes include a weak signal of RBM (Figure 1c). Before we discuss the detailed results obtained in our studies, it is useful to provide a general description of the CNT array growth kinetics.

Generalized Kinetic Formulation of Carbon Nanotube Array Growth. The CVD synthesis of carbon nanotubes involves a series of transport and conversion events that produce a flux of carbon material from a precursor provided by the feed gases (or generated by a gas phase reaction) to the carbon nanotube growing from a catalyst particle site on the surface (Figure 2a,b). We can represent this series of events using a rather simple equivalent electrical circuit (Figure 2c), which includes contributions from three resistances: diffusion of the gas species through the growing CNT forest to the catalyst site (R_1); the resistance associated with the carbon adsorption to the catalyst surface, any further reactions happening there, as well as the resistance for incorporation of carbon into a growing carbon nanotube (R_2). This key parameter encompasses all the effects associated with catalyst deactivation through various mechanisms. The last resistance term (R_3) is associated with the diffusion of carbon through the catalyst particle to the CNT growth site.

Then if the driving force for the reactions we can write the rate of the CNT growth as

$$v_{gr} = \frac{\frac{\Delta\mu}{kT} n_0 \omega}{R_1 + R_2 + R_3} \quad (1)$$

where $\Delta\mu/kT$ is the driving force for the reaction, the n_0 is the initial catalyst active sites concentration, and ω is the kinetic coefficient. If we write the diffusion terms explicitly as

$$R_1 = \frac{h(t)}{D_g} = \frac{\int_t^o v(t)\,dt}{D_g} \quad (2)$$

$$R_3 = \frac{l}{D} \quad (3)$$

where $h(t)$ is the height of the CNT array, l is the effective size of the catalyst particle, and D_g and D are the carbon diffusion coefficients in the gas phase and through the catalyst particle, respectively. Finally, we can write down the generalized expression for the growth rate as

$$v_{gr} = \frac{\frac{\Delta\mu}{KT} n_0 \omega}{\frac{\int_0^t v(t)\,dt}{D_g} + £(t) + \frac{l}{D}} \quad (4)$$

where the $£(t)$ is a model-dependent function that describes catalyst deactivation. Equation 4 has several interesting features. First, not surprisingly, it predicts that the initial growth rate of the carbon nanotube array is proportional to the driving force for the reaction, that is, to the first order to the rate of carbon precursor production in the gas phase. Second, it sets the maximum theoretically achievable growth rate as $v_{gr}^{max} = ((\Delta\mu/kT)\, n_0 \omega D)/l$, where the growth is limited exclusively by the diffusion of carbon through the catalyst particle assuming that the adsorption resistance is much smaller than the diffusion resistance. Third, it predicts several kinetic regimes for the growth process depending on the relative value of the terms in the denominator of eq 4 (or eq 1). When $R_1 \gg R_2$, which corresponds to the growth limited by the diffusion of the precursor through the CNT array, the equation reduces to the Deal–Grove equation (see Supporting Information for details) that is often used to describe diffusion-limited CNT array growth.[27] When $R_1 \ll R_2$, then the growth is primarily limited by the catalyst deactivation process, and the kinetic can follow different law depending on the specific model of deactivation. For example, using the Kolmogorov–Mehl–Avrami model

to describe deactivation by carbon encapsulation reproduces the characteristic abrupt termination kinetics (see Supporting Information for details) that was seen in a number of studies.[14,21,28]

Finally, the initial growth rate could depend on the gas phase pyrolysis equilibrium that produces the active precursor, C_a, for the CNT synthesis. The simplest case assumes that the consumption of active carbon precursor by the growing nanotube does not change the steady state concentration of that precursor; then this equilibrium could be described by the following generalized kinetic equations:

$$\frac{d[C_a]}{dt} = k_1[C_2H_4] - k_2[H_2][C_a] \quad (5)$$

$$v_g^0 \sim [C_a] = K\frac{[C_2H_4]}{[H_2]}(1 - e^{-k_2\tau_r[H_2]}) \quad (6)$$

where $K = k_1/k_2$ and τ_r is the reaction time, determined mostly by the dynamics of gas flow through the CVD reactor. In the quasi-stationary case eq 6 reduces to

$$v_g^0 \sim [C_a] = K\frac{[C_2H_4]}{[H_2]} \quad (7)$$

Initial Growth Rate. All growth runs were characterized by the kinetics that exhibited three common regimes (Figure 1f): the rate would initially show a rapid decay, then a relatively slow monotonous decrease, followed by abrupt termination. Note that the superior time resolution provided by the *in situ* monitoring system is critical to discern these features. The CNT growth kinetics is often described by the exponential decay model (also commonly known as lijima's model).[29] Figure 1f shows that this model does not capture the three different regimes of the growth rate throughout the process; yet that model provides a seemingly adequate fit to the array height data (Figure 1f, inset) that is typically captured by an *ex-situ* analysis. In most cases the CNT growth rates decreased throughout the process, (Figure 3); except the very first moments of growth, where we often observed an induction period region (see for instance, the first growth curve (100 sccm of ethylene) in Figure 3a). Latorre *et al.*[30] suggested a phenomenological model attributing that initial induction period to the catalyst carburization. In contrast, Sharma *et al.*[31] used *in situ* TEM data to propose that CNT growth was always preceded by rapid cementite (Fe_3C) formation (<0.11 s). Our experiment did not provide a definitive answer to the origin of this behavior, as we could not exclude transient behaviors associated with imperfect gas mixing, alignment errors of the optical system, or a nonuniform initial growth rate. Therefore, all further analysis excludes initial transient region.

First, we examine the effect of the varying ethylene gas concentration from 5% to 60% at 750 °C while maintaining a 40% hydrogen concentration in the mixture (Figure 3a). The initial growth rates measured in these experiments were clearly proportional to the ethylene concentration (Figure 4a), which is consistent with the trends reported by other *in situ* studies.[32,33] The linear relation between the growth rates and ethylene concentration agrees with the predictions of eq 4, 6, and 7. The absence of the saturation behavior also suggests that the active carbon coverage on the catalyst was relatively small and that the (initial) growth was not limited by postadsorption processes.

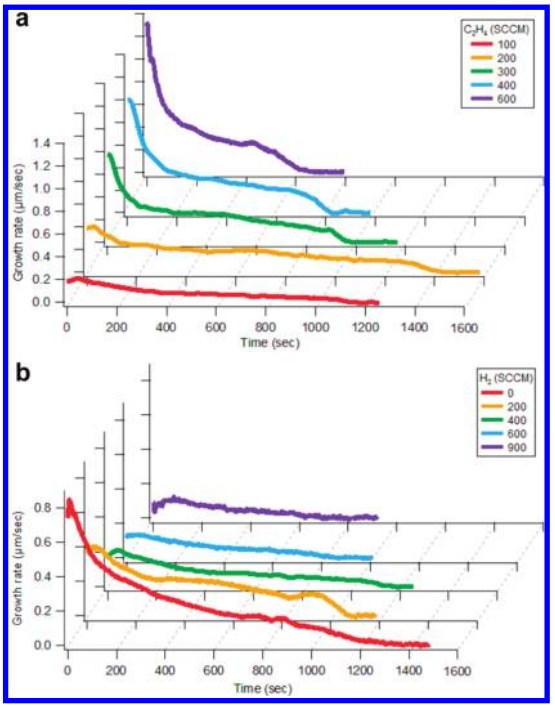

Figure 3. Representative growth rate curves obtained for runs with (a) fixed hydrogen flow of 400 SCCM and varying amounts of ethylene and (b) fixed ethylene flow of 100 SCCM and varying amounts of hydrogen. For all runs the total gas flow was maintained at 1000 SCCM and the growth temperature was 750 °C.

Another growth runs series conducted at the same condition but using varying amounts of hydrogen and a fixed ethylene concentration at 10% showed a monotonous decrease of the growth rate with the increase in hydrogen concentration (Figures 3b and 4b). Generally, we could attribute this behavior either to a shift of the gas phase reaction equilibrium, or to the influence of hydrogen on the reaction equilibrium at the catalyst surface. The most obvious possibility is that the addition of hydrogen to the system shifts the carbon production in the gas phase toward the reagents, thus decreasing the overall driving force for the process. In this case the reaction equilibrium will follow eq 6 and eq 7. Note that while eq 7, which is valid when the gas phase reaction reaches an equilibrium state, predicts a very simple inverse dependency of the growth rates on the hydrogen concentration, a more general eq 6 predicts a more complicated form. The experimental data (Figure 4b) show that while the

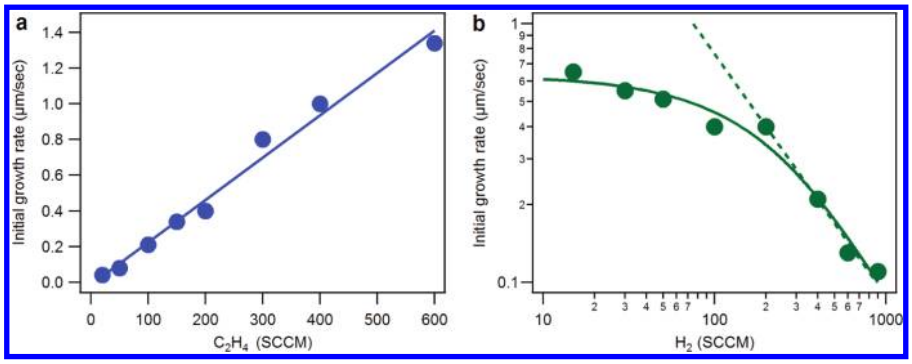

Figure 4. Initial growth rates as a function of (a) ethylene concentration and (b) hydrogen concentration in the gas mixture. Solid lines correspond to the fit in eq 6. Dotted line in panel b corresponds to the fit in eq 7.

kinetics follows the simpler eq 7 at high hydrogen concentrations (Figure 4b, dotted line), it clearly diverges at lower hydrogen concentrations. Instead, the complete data set is much better described by eq 6 (Figure 4b, solid line). This data strongly suggests that one of the main roles of hydrogen in our CVD process is shifting the pyrolysis equilibrium of ethylene and that at least at low hydrogen concentrations the gas pyrolysis equilibrium keeps shifting as the gas travels through the reactor tube. This conclusion is also consistent with the strong dependence on the reaction rate on the overall gas flow rate in the system (see Figure S4, S5 in Supporting Information), as well as the literature reports on the importance of the "dwell time" of hydrocarbon gas in the hot wall reactor for optimizing CNT growth.[34] Interestingly, the gas phase equilibrium in this system may be more complex than what is described by eq 6, as the flow rate data indicate that the gas pyrolysis equilibrium keeps shifting even at relatively high hydrogen concentrations.

While the decrease in growth rate can be attributed to etching of a growing carbon nanotube by hydrogen,[35] our experimental observation does not support this idea. When we exposed the partially grown CNT array to 40% of hydrogen diluted with helium for 1 h at the growth temperature (750 °C), we could not detect any measurable changes in the CNT array height. This result suggests that any nanotube etching by adsorbed hydrogen or possibly desorbed atomic hydrogen is either nonexistent or at least very slow[16,36] in our growth conditions.

Activation Energy. Estimates of the apparent activation energy (E_a) from an Arrhenius equation ($v_g \approx e^{-E_a/RT}$) often help to identify a rate-limiting step in the overall growth kinetics. To obtain this value we conducted a series of growth runs at different temperatures using 10% C_2H_4/40% H_2 process gas mixture. The initial growth rates obtained in these measurements were well described by the Arrhenius equation with an activation energy of about 2.6 eV (Figure 5). This value is quite similar to the activation energy of 2.8 eV reported by Yasuda *et al.* for a similar CNT growth process.[34] Notably, this energy is considerably higher

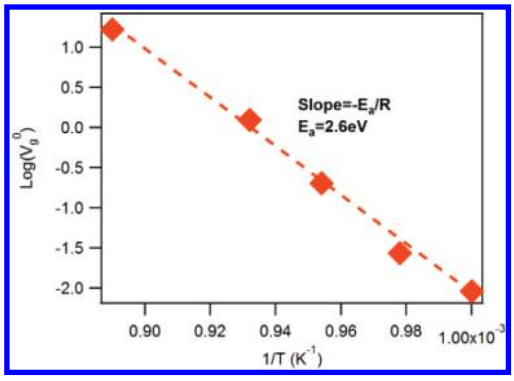

Figure 5. Arrhenius plot of the initial growth rate as a function of temperature. Feed gas composition was 100 C_2H_4/400 H_2/500 He (all flows in SCCM.).

than a typical energy for the bulk diffusion (1−1.7 eV)[36] and surface diffusion (0.23−0.4 eV)[37] of carbon. Surface reaction processes of carbon feedstock are characterized by the activation barrier of 1.66 eV for acetylene−Fe[38] and 2.0 eV with ethylene−Fe[39] systems. Gas phase diffusion is typically a very rapid process with much lower activation energy; therefore it is unlikely that the *initial* growth is limited by mass transport of ethylene molecules. Picher *et al.*[33] observed similar activation energy values (2.8 eV for Ni, 2.4 eV for Co), but they used ethanol as a carbon source and attributed the high activation energy to a particular mechanism of ethanol decomposition. The only other possibility that we could consider is that a gas phase reaction (GPR) that generates active precursors for the CNT synthesis is responsible for the high activation energy value.

This argument has an essential implication on the role of GPR; the active precursor of GPR should be efficient enough to neglect direct contribution of the original hydrocarbon, ethylene in our case. Literature reports also point to the existence of several efficient precursors for nanotube growth. Several pyrolysis products appear to be more efficient growth agents than the original carbon feedstock: for instance, benzene,[9] acetylene,[8,10,11] and C_4H_4.[15] Especially, Eres *et al.*[40] demonstrated that nanotube growth yield of acetylene is remarkably higher than other hydrocarbons

when they prevented any possible gas phase reactions with their molecular beam growth system. Moreover, acetylene produced nanotube growth in those conditions, while ethylene produced no carbon deposit. Indeed, a simple estimate of the sticking probability gives additional support to the importance of acetylene for this reaction and to the assumption that gas phase reaction plays a significant role in CNT synthesis. If we compare our CNT growth rate with the flux of ethylene molecule impinging the surface, we estimate that the sticking probability is only about 10^{-5} at 1023 K. However, Gamalski *et al.*[41] reported a much higher sticking probability of 0.042−0.2 for acetylene. Considering that acetylene is one of the products of the ethylene pyrolysis near 1000 K,[42] it is likely that generation of acetylene in the gas phase reaction is the key component of the growth mechanism.

Further reactions from the product acetylene may involve more complicated chemistry that possibly affects growth;[15] however, we focus on the role of acetylene and assume that acetylene is either the real precursor or chemical intermediate close to that precursor. Even though we could not rigorously identify the real precursor, the ethylene-to-acetylene reaction can reasonably explain our growth kinetics with ethylene carbon feedstock.

In addition, we speculate that the GPR is likely assisted by some reactive products desorbing from the catalyst. Similar catalyst-assisted preconditioning of CVD precursor was reported in GaP nanowire growth, where trimethylgallium evolved into monomethylgallium stepwise with the help of Au catalyst.[43] Graphene growth studies by CVD also reported that the preconditioning of the upstream gas by a copper catalyst promotes formation of bilayer Bernal graphene that is placed downstream.[44] Indeed our studies show evidence that the same preconditioning scheme with an active upstream catalyst promotes growth of carbon nanotubes on the downstream substrate (see Figure S3, Supporting Information).

Catalyst Lifetime and Growth Termination. Another key parameter for the CNT growth characterization of the catalyst lifetime, defined as the time it takes the growing array to reach the termination stage (for practical reasons we define that time as the time beyond which growth rate decays below 0.01 μm/sec). Researchers have proposed several termination mechanisms for the CVD growth of CNT arrays. Nanotube growth can be stopped by excessive amorphous or graphitic carbon,[21,45] encapsulating active sites on catalyst. If this is the case, catalyst can be regenerated by carbon etchant, specifically oxygen-containing molecules.[10,45] Catalyst may be deactivated by Ostwald ripening, which could also be partially suppressed by water.[5] Finally, growth rate can be diminished by growing nanotube forest since it acts as a diffusion barrier when catalyst particle remain at the root of

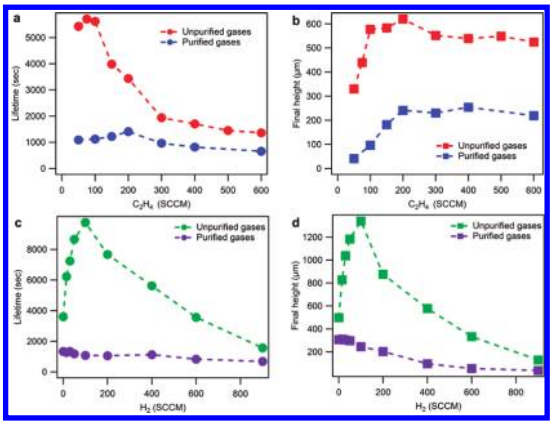

Figure 6. Growth lifetime (a,c) and final height of the CNT arrays (b,d) as a function of the ethylene and hydrogen content of the feed gas mixture, and the degree of gas purification. For the ethylene content variation series the hydrogen flow was always 400 SCCM, and for the hydrogen variations series the ethylene flow was fixed at 100 SCCM. In all experiments the helium flow rate was adjusted to keep the total flow rate at 1000 SCCM for all cases. Kinetic trends for the unpurified gases were taken from a previous study.[12]

nanotubes and the forest grows thicker; then catalyst patterning will facilitate better gas diffusion.[27] Nevertheless, none of these mechanisms has been solely established as the dominating cause of growth termination; rather, a particular termination mechanism manifests itself more apparently at a biased condition, or multiple reasons are responsible in a combined way depending on the parametric window of the experiments. In this study, we focus on growth termination especially with dedicated efforts to purify (or deoxidize) the process gases that result in remarkably different trend. Typically, CVD growth experiments done with laboratory-grade purity gases produce a complicated trend in catalyst lifetime as a function of the gas mixture composition (Figure 6a,c). For example, from measurements using standard ultrahigh purity gases,[25] the catalyst lifetime first show a brief increase and then a steady significant decrease as a function of the carbon feedstock concentration (Figure 6a). The increase in hydrogen concentration leads to the very sharp increase in the catalyst lifetime followed by a significant decline. As we reported recently most of these trends originate in the complicated effects of the impurities in the feed gases.[24] Indeed, when we repeated this growth using purified gases, most of the complicated trends have vanished revealing starkly simple kinetics.

The most unexpected result from these experiments is the almost complete insensitivity of the growth lifetime to the changes in the carbon concentration and hydrogen concentration. If the carbon encapsulation mechanism is the dominating mechanism for growth termination, then the process should be very sensitive to the carbon concentration on catalyst surface (and in the gas phase);[21,45,46] the experimental

data clearly do not support this conclusion. Similarly, considering that the increased hydrogen concentration suppresses the formation of the CNT growth precursors, then the level of hydrogen in the feed mixture should have a profound effect on the termination process; data on Figure 6c clearly show that it does not. Moreover, if the carbon encapsulation was a significant cause of the CNT growth stoppage, we should be able to regenerate "dead" catalyst by treating it with a carbon etchant, such as water vapor.[45] However in our experiments once the catalyst was completely deactivated we could not restart the growth; at best we could only regrow short collapsed nanotubes with very low yield after we removed the "dead" CNT array from the surface. These results argue strongly that carbon encapsulation is not the main cause of the VACNT array growth termination, at least for the growth conditions that produce abrupt terminations similar to the data on Figure 1f (even though the carbon termination model reproduces the shape of the kinetics curves well).[21] As we discussed in the previous sections, gradual terminations likely reflect the kinetics of diffusion-limited supply of carbon feedstock to the catalyst, and thus cannot provide much information about the termination process.

Another plausible reason for deactivation is the ripening of metal catalyst,[5] which is inevitable at high temperatures. Recently, Kim *et al.*[26] demonstrated by *in situ* TEM that catalyst ripening could lead to growth termination. They also showed those ripened catalyst particles eventually migrated into the alumina supporting layer and thereby became completely deactivated, which would explain irreversible loss of catalytic activity. To monitor the ripening behavior of catalyst in our experiments we exposed the catalyst to our standard clean hydrogen–helium pretreatment for 1 h longer than the 17 min total time that we used for a regular annealing recipe. Unlike the data observed in other studies,[5,26] the corresponding AFM images (Figure 7) do not show the dramatic change in the particle size and number density that would be representative of the ripening process. Moreover, when we

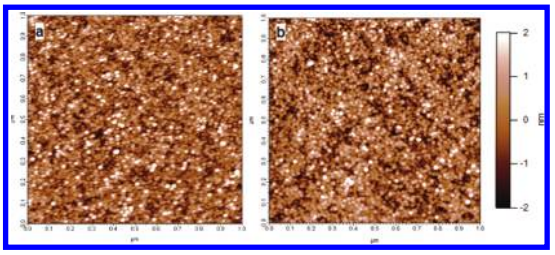

Figure 7. AFM images (a) after typical annealing procedure and (b) after additional 1 h annealing.

delayed the ethylene introduction time (thus allowing more annealing) we obtained growth rate curves that were almost identical to the rate curve obtained without such time delay (see Figure S2, Supporting Information). These results indicate that the catalyst deactivation kinetics does not follow a simply ripening process. Maruyama and co-workers have also estimated that the termination mechanism, which originates in the diffusion barrier through the growing CNT forest, also could not be rate-limiting.[47] The data on the Figure 6b, which show the clear saturation of the array final height with the carbon concentration increase, also argue against this mechanism.

What do our results tell us about the kinetics of "clean" VACNT forest growth and growth termination? First, they show that current hypotheses about the potential termination mechanism do not provide an adequate, comprehensive, and consistent explanation. Moreover, our data definitively rule out the mechanisms that have been dominating the literature—encapsulation of the catalyst by amorphous carbon. Second, they show that the growth kinetics follows very simple rule—the initial growth rate is always proportional to the concentration of the active carbon species. Third, and the most important result of this study is that the gas phase pyrolysis of carbon feedstock gas has a dominating effect on the growth kinetics in the hot wall reactor growth. Thus the future studies of the CNT growth have to pay the utmost attention to exploring and controlling this part of the growth process.

METHODS

Carbon Nanotube Growth Setup and Gas Purification Setup. Our home-built thermal CVD system consists of gas feeding system, high temperature furnace (Lindberg Blue TF55035A, Thermo Electron Corp.), and *in situ* measurement system. To introduce process gases, helium (purity: 99.999%), hydrogen (purity: 99.9999%), and ethylene (purity: 99.999%) cylinders were connected to mass flow controllers (MKS). Especially, we installed high-performance deoxo purifying units (PureGuard, Johnson Matthey) between the gas regulators of cylinders and flow controllers to further purify gases. A hygrometer (Hygrophil-F 5672, Bartec) was placed after the flow controllers to monitor water level in gases. Especially, we put a dedicated effort to maintain very dry gas lines. The flow lines were kept above 100 °C by a heat tape to prevent condensation of water. To minimize water introduction to the gas line, we applied a valve between the end of gas feed line and inlet of quartz tube (reactor tube) so that the valve was closed whenever the catalyst substrate was loaded or unloaded.

***In-Situ* Growth Kinetics Monitoring Setup.** To monitor the growth kinetics *in situ*, the furnace was equipped with an optical micrometer setup (LS7030M, Keyence) that uses a shadow of the growing CNT array projected onto a CCD chip to follow the growth process. To install, the optical micrometer parts of the furnace cover were removed since the micrometer's working distance is shorter than the furnace dimension. To reduce heat loss from the furnace and shield the measurement system, we also installed additional aluminum covers with heat absorbing windows (Schott KG Heat Absorbing Glass, Edmund Optics Inc.) Kinetic data was logged every second from 1 min before ethylene

introduction to the end of growth using the built-in capabilities of the system.

Substrate Preparation and Catalyst Deposition. Before catalyst deposition, a silicon wafer (100) was half-diced (~250 μm in depth) to get a regular size (5 mm × 5 mm) of substrate pieces. To protect the silicon surface from chip deposit during the dicing process, 100 nm of sacrificial photoresist was coated, which would be removed by the Plasma PR removing system (Matrix Asher Model 106) before catalyst deposition. Double layers of iron (2 nm)/alumina (30 nm) were used as catalyst. Alumina was deposited by RF sputtering (Edwards Auto 306 DC and RF Sputter Coater) with an alumina target (Plasmaterials, Inc.) For iron deposition, the e-beam evaporator (Edwards EB3 Electron Beam Evaporator) was used with the metal iron target (Plasmaterials, Inc.). The deposition rates were kept slow (~0.5 nm/min for alumina and ~0.3 nm/min for iron) to achieve uniform and controllable film thickness. After the catalyst deposition, the half-diced wafer was split into individual chips (5 mm × 5 mm) by applying moderate force.

CNT Array Growth. Before every run of CVD growth, the quartz tube was heated at 850 °C for 10 min with exposure to atmosphere so as to remove any carbon residue in the tube. While cooling the furnace after this cleaning step, we closed the open tube when it reached 500 °C. After loading a catalyst substrate at below 100 °C, we purged the system for an additional 10 min with 1000 SCCM of helium to remove any possible gases introduced from the ambient. The total pressure was maintained at 1 atm for all of the experiments. The first heat-up rate was 50 °C/min and the second ramp-up was from 725 °C to a growth temperature (T_g) for 1 min. Before growth was initiated by ethylene, catalyst was annealed with a mixture gas of hydrogen and helium to reduce the oxide of the Fe catalyst into a metallic form; 40% (400 SCCM) hydrogen was introduced when the temperature for the first ramp-up reached 550 °C. The hydrogen flow was maintained by the end of first annealing step (12 min), and then it was reduced to 15 SCCM for 5 min. Finally, when growth was initiated by ethylene introduction, a gas mixture of ethylene, hydrogen, and helium was introduced. After termination of the growth, the as-grown nanotube chip was unloaded when the temperature went below 350 °C in order to prevent nanotubes from being thermally damaged by air. The CVD growth process is summarized in the Supporting Information (Figure S1).

Acknowledgment. The authors thank Xiang Bin for TEM imaging of nanotubes. J.I. thanks Kang Rae Cho for valuable discussion. All authors thank the anonymous reviewer for helpful and insightful comments. Research was supported by National Science Foundation NIRT CBET-0709090 (A.N., C.G., and J.B.I.). A.N. was supported by the U.S. Department of Energy, Office of Basic Energy Sciences, Division of Materials Sciences and Engineering. Work at the Molecular Foundry was supported by the Office of Science, Office of Basic Energy Sciences, of the U.S. Department of Energy under Contract No. DE-AC02-05CH11231. Parts of the work were performed under the auspices of the U.S. Department of Energy by Lawrence Livermore National Laboratory under Contract DE-AC52-07NA27344.

Supporting Information Available: Additional data and figures as described in the text. This material is available free of charge *via* the Internet at http://pubs.acs.org.

REFERENCES AND NOTES

1. Fan, S. S.; Chapline, M. G.; Franklin, N. R.; Tombler, T. W.; Cassell, A. M.; Dai, H. J. Self-Oriented Regular Arrays of Carbon Nanotubes and Their Field Emission Properties. *Science* **1999**, *283*, 512–514.
2. Holt, J. K.; Park, H. G.; Wang, Y.; Stadermann, M.; Artyukhin, A. B.; Grigoropoulos, C. P.; Noy, A.; Bakajin, O. Fast Mass Transport through Sub-2-nanometer Carbon Nanotubes. *Science* **2006**, *312*, 1034–1037.
3. Hafner, J. H.; Bronikowski, M. J.; Azamian, B. R.; Nikolaev, P.; Rinzler, A. G.; Colbert, D. T.; Smith, K. A.; Smalley, R. E. Catalytic Growth of Single-Wall Carbon Nanotubes from Metal Particles. *Chem. Phys. Lett.* **1998**, *296*, 195–202.
4. Hata, K.; Futaba, D. N.; Mizuno, K.; Namai, T.; Yumura, M.; Iijima, S. Water-Assisted Highly Efficient Synthesis of Impurity-Free Single-Waited Carbon Nanotubes. *Science* **2004**, *306*, 1362–1364.
5. Amama, P. B.; Pint, C. L.; McJilton, L.; Kim, S. M.; Stach, E. A.; Murray, P. T.; Hauge, R. H.; Maruyama, B. Role of Water in Super Growth of Single-Walled Carbon Nanotube Carpets. *Nano Lett.* **2009**, *9*, 44–49.
6. Yasuda, S.; Futaba, D. N.; Yamada, T.; Satou, J.; Shibuya, A.; Takai, H.; Arakawa, K.; Yumura, M.; Hata, K. Improved and Large Area Single-Walled Carbon Nanotube Forest Growth by Controlling the Gas Flow Direction. *ACS Nano* **2009**, *3*, 4164–4170.
7. Patole, S. P.; Kim, H.; Choi, J.; Kim, Y.; Baik, S.; Yoo, J. B. Kinetics of Catalyst Size Dependent Carbon Nanotube Growth by Growth Interruption Studies. *Appl. Phys. Lett.* **2010**, *96*, 094101.
8. Zhong, G.; Hofmann, S.; Yan, F.; Telg, H.; Warner, J. H.; Eder, D.; Thomsen, C.; Milne, W. I.; Robertson, J. Acetylene: A Key Growth Precursor for Single-Walled Carbon Nanotube Forests. *J. Phys. Chem. C* **2009**, *113*, 17321–17325.
9. Franklin, N. R.; Dai, H. J. an Enhanced Cvd Approach to Extensive Nanotube Networks with Directionality. *Adv. Mater.* **2000**, *12*, 890–894.
10. Futaba, D. N.; Goto, J.; Yasuda, S.; Yamada, T.; Yumura, M.; Hata, K. General Rules Governing the Highly Efficient Growth of Carbon Nanotubes. *Adv. Mater.* **2009**, *21*, 4811–4815.
11. Bell, M. S.; Lacerda, R. G.; Teo, K. B. K.; Rupesinghe, N. L.; Amaratunga, G. A. J.; Milne, W. I.; Chhowalla, M. Plasma Composition during Plasma-Enhanced Chemical Vapor Deposition of Carbon Nanotubes. *Appl. Phys. Lett.* **2004**, *85*, 1137–1139.
12. Qian, W. Z.; Tian, T.; Guo, C. Y.; Wen, Q.; Li, K. J.; Zhang, H. B.; Shi, H. B.; Wang, D. Z.; Liu, Y.; Zhang, Q.; *et al*. Enhanced Activation and Decomposition of CH_4 by the Addition of C_2H_4 or C_2H_2 for Hydrogen and Carbon Nanotube Production. *J. Phys. Chem. C* **2008**, *112*, 7588–7593.
13. Ma, H.; Pan, L.; Nakayama, Y. Influence of Gas-Phase Reactions on the Growth of Carbon Nanotubes. *J. Phys. Chem. C* **2010**, *114*, 2398–402.
14. Meshot, E. R.; Hart, A. J. Abrupt Self-Termination of Vertically Aligned Carbon Nanotube Growth. *Appl. Phys. Lett.* **2008**, *92*, 113107.
15. Plata, D. e. L.; Meshot, E. R.; Reddy, C. M.; Hart, A. J.; Gschwend, P. M. Multiple Alkynes React with Ethylene To Enhance Carbon Nanotube Synthesis, Suggesting a Polymerization-like Formation Mechanism. *ACS Nano* **2010**, *4*, 7185–7192.
16. Pirard, S. L.; Douven, S.; Bossuot, C.; Heyen, G.; Pirard, J. P. A Kinetic Study of Multi-walled Carbon Nanotube Synthesis by Catalytic Chemical Vapor Deposition Using a Fe-Co/Al_2O_3 Catalyst. *Carbon* **2007**, *45*, 1167–1175.
17. Behr, M. J.; Gaulding, E. A.; Mkhoyan, K. A.; Aydil, E. S. Effect of Hydrogen on Catalyst Nanoparticles in Carbon Nanotube Growth. *J. Appl. Phys.* **2010**, *108*, 053303.
18. Okita, A.; Suda, Y.; Oda, A.; Nakamura, J.; Ozeki, A.; Bhattacharyya, K.; Sugawara, H.; Sakai, Y. Effects of Hydrogen on Carbon Nanotube Formation in CH_4/H_2 Plasmas. *Carbon* **2007**, *45*, 1518–1526.
19. Nessim, G. D.; Hart, A. J.; Kim, J. S.; Acquaviva, D.; Oh, J. H.; Morgan, C. D.; Seita, M.; Leib, J. S.; Thompson, C. V. Tuning of Vertically-Aligned Carbon Nanotube Diameter and Areal Density through Catalyst Pre-treatment. *Nano Lett.* **2008**, *8*, 3587–3593.
20. Bedewy, M.; Meshot, E. R.; Guo, H.; Verploegen, E. A.; Lu, W.; Hart, A. J. Collective Mechanism for the Evolution and Self-Termination of Vertically Aligned Carbon Nanotube Growth. *J. Phys. Chem. C* **2009**, *113*, 20576–20582.
21. Stadermann, M.; Sherlock, S. P.; In, J.; Fornasiero, F.; Dick, B. A.; Park, H. G.; Artyukhin, A. B.; Wang, Y.; De Yoreo, J. J.; Grigoropoulos, C. P.; Bakajin, O.; Chernov, A. A.; Noy, A. Length Control and Catalyst Poisoning in CVD Growth of Multi-wall Carbon Nanotube Arrays. *Nano Lett.* **2009**, *9*, 738–744.

22. Han, J. H.; Graff, R. A.; Welch, B.; Marsh, C. P.; Franks, R.; Strano, M. S.; Mechanochemical, A. Model of Growth Termination in Vertical Carbon Nanotube Forests. *ACS Nano* **2008**, *2*, 53–60.
23. Pint, C. L.; Pheasant, S. T.; Parra-Vasquez, A. N. G.; Horton, C.; Xu, Y. Q.; Hauge, R. H. Investigation of Optimal Parameters for Oxide-Assisted Growth of Vertically Aligned Single-Walled Carbon Nanotubes. *J. Phys. Chem. C* **2009**, *113*, 4125–4133.
24. In, J. B.; Grigoropoulos, C. P.; Chernov, A. A.; Noy, A. Hidden Role of Trace Gas Impurities in Chemical Vapor Deposition Growth of Vertically-Aligned Carbon Nanotube Arrays. *Appl. Phys. Lett.* **2011**, *98*, 153102.
25. Yasuda, S.; Futaba, D. N.; Yumura, M.; Iijima, S.; Hata, K. Diagnostics and Growth Control of Single-Walled Carbon Nanotube Forests Using a Telecentric Optical System for *in Situ* Height Monitoring. *Appl. Phys. Lett.* **2008**, *93*, 143115.
26. Kim, S. M.; Pint, C. L.; Amama, P. B.; Zakharov, D. N.; Hauge, R. H.; Maruyama, B.; Stach, E. A. Evolution in Catalyst Morphology Leads to Carbon Nanotube Growth Termination. *J. Phys. Chem. Lett.* **2010**, *1*, 918–922.
27. Zhong, G. F.; Iwasaki, T.; Robertson, J.; Kawarada, H. Growth Kinetics of 0.5 cm Vertically Aligned Single-Walled Carbon Nanotubes. *J. Phys. Chem. B* **2007**, *111*, 1907–1910.
28. Puretzky, A. A.; Eres, G.; Rouleau, C. M.; Ivanov, I. N.; Geohegan, D. B. Real-Time Imaging of Vertically Aligned Carbon Nanotube Array Growth Kinetics. *Nanotechnology* **2008**, *19*, 55605–55610.
29. Futaba, D. N.; Hata, K.; Yamada, T.; Mizuno, K.; Yumura, M.; Iijima, S. Kinetics of Water-Assisted Single-Walled Carbon Nanotube Synthesis Revealed by a Time-Evolution Analysis. *Phys. Rev. Lett.* **2005**, *95*, 056104–056109.
30. Latorre, N.; Romeo, E.; Cazana, F.; Ubieto, T.; Royo, C.; Villacampa, J. J.; Monzon, A. Carbon Nanotube Growth by Catalytic Chemical Vapor Deposition: A Phenomenological Kinetic Model. *J. Phys. Chem. C* **2010**, *114*, 4773–4782.
31. Sharma, R.; Moore, E.; Rez, P.; Treacy, M. M. J. Site-Specific Fabrication of Fe Particles for Carbon Nanotube Growth. *Nano Lett.* **2009**, *9*, 689–694.
32. Einarsson, E.; Murakami, Y.; Kadowaki, M.; Maruyama, S. Growth Dynamics of Vertically Aligned Single-Walled Carbon Nanotubes from *in Situ* Measurements. *Carbon* **2008**, *46*, 923–930.
33. Picher, M.; Anglaret, E.; Arenal, R.; Jourdain, V. Self-Deactivation of Single-Walled Carbon Nanotube Growth Studied by *in Situ* Raman Measurements. *Nano Lett.* **2009**, *9*, 542–547.
34. Yasuda, S.; Futaba, D. N.; Yamada, T.; Yumura, M.; Hata, K. Gas Dwell Time Control for Rapid and Long Lifetime Growth of Single-Walled Carbon Nanotube Forests. *Nano Lett.* **2011**, *11*, 3617–3623.
35. Zhang, G. Y.; Mann, D.; Zhang, L.; Javey, A.; Li, Y. M.; Yenilmez, E.; Wang, Q.; McVittie, J. P.; Nishi, Y.; Gibbons, J.; Dai, H. J. Ultra-High-Yield Growth of Vertical Single-Walled Carbon Nanotubes: Hidden Roles of Hydrogen and Oxygen. *Proc. Natl. Acad. Sci. U.S.A.* **2005**, *102*, 16141–16145.
36. Wirth, C. T.; Zhang, C.; Zhong, G. F.; Hofmann, S.; Robertson, J. Diffusion- and Reaction-Limited Growth of Carbon Nanotube Forests. *ACS Nano* **2009**, *3*, 3560–3566.
37. Hofmann, S.; Csanyi, G.; Ferrari, A. C.; Payne, M. C.; Robertson, J. Surface Diffusion: The Low Activation Energy Path for Nanotube Growth. *Phys. Rev. Lett.* **2005**, *95*, 036101/1–4.
38. Liu, K.; Jiang, K. L.; Feng, C.; Chen, Z.; Fan, S. S.; Growth Mark, A Method for Studying Growth Mechanism of Carbon Nanotube Arrays. *Carbon* **2005**, *43*, 2850–2856.
39. Bronikowski, M. J. Longer Nanotubes at Lower Temperatures: The Influence of Effective Activation Energies on Carbon Nanotube Growth by Thermal Chemical Vapor Deposition. *J. Phys. Chem. C* **2007**, *111*, 17705–17712.
40. Eres, G.; Kinkhabwala, A. A.; Cui, H. T.; Geohegan, D. B.; Puretzky, A. A.; Lowndes, D. H. Molecular Beam-Controlled Nucleation and Growth of Vertically Aligned Single-Wall Carbon Nanotube Arrays. *J. Phys. Chem. B* **2005**, *109*, 16684–16694.
41. Gamalski, A.; Moore, E. S.; Treacy, M. M. J.; Sharma, R.; Rez, P. Diffusion-Gradient-Induced Length Instabilities in the Catalytic Growth of Carbon Nanotubes. *Appl. Phys. Lett.* **2009**, *95*, 233109–233112.
42. Roscoe, J. M.; Bossard, A. R.; Back, M. H. A Kinetic Modeling Study of Ethylene Pyrolysis. *Can. J. Chem.—Rev. Can. Chim.* **2000**, *78*, 16–25.
43. Borgstrom, M. T.; Immink, G.; Ketelaars, B.; Algra, R.; Bakkers, E. Synergetic nanowire growth. *Nat. Nanotechnol.* **2007**, *2*, 541–544.
44. Yan, K.; Peng, H. L.; Zhou, Y.; Li, H.; Liu, Z. F. Formation of Bilayer Bernal Graphene: Layer-by-Layer Epitaxy *via* Chemical Vapor Deposition. *Nano Lett.* **2011**, *11*, 1106–1110.
45. Yamada, T.; Maigne, A.; Yudasaka, M.; Mizuno, K.; Futaba, D. N.; Yumura, M.; Iijima, S.; Hata, K. Revealing the Secret of Water-Assisted Carbon Nanotube Synthesis by Microscopic Observation of the Interaction of Water on the Catalysts. *Nano Lett.* **2008**, *8*, 4288–4292.
46. Lee, D. H.; Kim, S. O.; Lee, W. J. Growth Kinetics of Wall-Number Controlled Carbon Nanotube Arrays. *J. Phys. Chem. C* **2010**, *114*, 3454–3458.
47. Xiang, R.; Yang, Z.; Zhang, Q.; Luo, G. H.; Qian, W. Z.; Wei, F.; Kadowaki, M.; Einarsson, E.; Maruyama, S. Growth Deceleration of Vertically Aligned Carbon Nanotube Arrays: Catalyst Deactivation or Feedstock Diffusion Controlled? *J Phys. Chem. C* **2008**, *112*, 4892–4896.